Cluster Compounds

Deutsche Ausgabe: DOI: 10.1002/ange.201601134
Internationale Ausgabe: DOI: 10.1002/anie.201601134

Amphoteric Aqueous Hafnium Cluster Chemistry

*Sara Goberna-Ferrón, Deok-Hie Park, Jenn M. Amador, Douglas A. Keszler, and May Nyman**

Abstract: *Selective dissolution of hafnium-peroxo-sulfate films in aqueous tetramethylammonium hydroxide enables extreme UV lithographic patterning of sub-10 nm HfO_2 structures. Hafnium speciation under these basic conditions (pH > 10), however, is unknown, as studies of hafnium aqueous chemistry have been limited to acid. Here, we report synthesis, crystal growth, and structural characterization of the first polynuclear hydroxo hafnium cluster isolated from base, $[TMA]_6[Hf_6(\mu\text{-}O_2)_6(\mu\text{-}OH)_6(OH)_{12}]\cdot 38\,H_2O$. The solution behavior of the cluster, including supramolecular assembly via hydrogen bonding is detailed via small-angle X-ray scattering (SAXS) and electrospray ionization mass spectrometry (ESI-MS). The study opens a new chapter in the aqueous chemistry of hafnium, exemplifying the concept of amphoteric clusters and informing a critical process in single-digit-nm lithography.*

Water-soluble molecular oxo-hydroxo metal clusters are recognized building blocks for deposition of functional thin-film coatings, offering low energy and "green" processing.[1–3] Additionally, selected hafnium-peroxo-sulfate clusters provide unprecedented dimensional control in nanolithography.[4,5] In this lithography, unexposed oxo-hydroxo Hf regions dissolve in base, meaning soluble hafnium species exist at high pH.

Up to now, however, the aqueous chemistry of hafnium has been documented only for strongly acidic conditions. In mildly acidic conditions (pH ≥ 3), gels and precipitates result from rapid hydrolysis and condensation.[6,7] At low pH, oxo-hydroxo hafnium clusters are commonly stabilized and isolated with capping sulfate ligands, sometimes linking clusters into 1, 2 or 3-dimensional networks.[7] These clusters include $Hf_{18}O_{10}(OH)_{26}(SO_4)_{13}(H_2O)_{33}$,[8] $[Hf_{17}O_8(OH)_{28}(SO_4)_{11}(H_2O)_{23}]^{2+}$,[9] $[Hf_{11}O_7(OH)_{11}(SO_4)_{15}(H_2O)_6]^{11-}$,[7] $[Hf_9O_8(OH)_6(SO_4)_{14}]^{14-}$,[10] and $[Hf_6O_5(SO_4)_{10.5}(H_2O)_{6.5}]^{7-}$.[7,11] The only reported sulfate-free cluster is the tetrameric species $[Hf_4(OH)_8(H_2O)_{16}]^{8+}$, commonly known as $HfOCl_2\cdot x\,H_2O$.[12,13]

Our interest in oxo-hydroxo hafnium speciation in base arises from the development step in lithographic patterning with the water-processed hafnium material known as $HafSO_x$, formulated $Hf_4(OH)_{6.4}(O_2)_2(SO_4)_{2.8}$.[4,5,14] Nanolithography allows bulk semiconductors and metals to be shaped into computing devices with sub-10 nm features.[15] New inorganic resists, such as $HafSO_x$, offer ultra-high-resolution patterns.[6] There are two major steps in the patterning process with HafSOx: 1) exposure, which causes dissociation of the peroxo ligand and induces condensation; and 2) development, where unexposed material is selectively dissolved in concentrated aqueous tetramethylammonium hydroxide (TMAH). The nature of the species produced in these basic solutions is unknown. This dissolution, coupled with stability of a similar peroxo-phosphato-niobium cluster observed in both basic and acidic solutions[16] has led us to propose the concept of *amphoteric clusters*, wherein simple ligand sets stabilize a single cluster or similar clusters at the extreme ends of the pH scale. This concept broadens the approach to cluster synthesis and study, as most common cluster types exist across limited pH ranges.[17] For example, Group 13 polycations are currently known to exist in the narrow range pH 3–4;[18,19] V, Mo, and W polyoxometalates (POMs), pH ≈ 1–7; and Nb and Ta POMs, pH > 10.[20–23]

Herein, we report the synthesis and structure of the peroxo-hydroxo-hafnium cluster $[TMA]_6[Hf_6(\mu\text{-}O_2)_6(\mu\text{-}OH)_6(OH)_{12}]\cdot 38\,H_2O$ (**Hf_6**), the first example of a hydroxo hafnium cluster isolated in base. The cluster contains bridging hydroxy ligands, like hafnium clusters in acid. **Hf_6** presents a rare feature of terminal hydroxy ligands. These ligands are commonly reactive toward condensation, thereby limiting cluster isolation. The H-bond effects of these reactive ligands in both solution and solid-state are documented by structure analysis, small angle X-ray scattering (SAXS), and electrospray-ionization mass spectrometry (ESI-MS).

The structure of **Hf_6** (Figure 1), established by X-ray crystallographic analysis,[24] exhibits a hexanuclear peroxo-hydroxo-Hf polyanion. Neighboring eight-coordinate Hf atoms link via one μ-peroxo and one μ-hydroxo ligand, forming a ring.

Each Hf atom completes its coordination sphere with two terminal hydroxo groups. The H atoms of these hydroxo

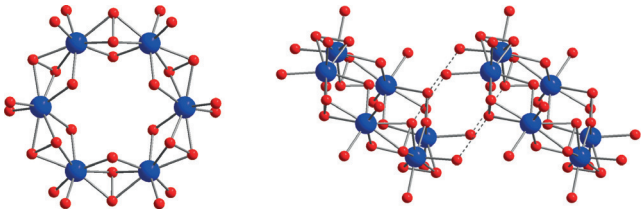

Figure 1. Structure of the **Hf_6** cluster $Hf_6(\mu\text{-}O_2)_6(\mu\text{-}OH)_6(OH)_{12}]^{6-}$ (left) and illustration of intermolecular hydrogen bonds (right). Blue spheres: Hf, red spheres: O. Hydrogens were not found directly, but inferred by charge-balance and BVS (see text).

[*] Dr. S. Goberna-Ferrón, D.-H. Park, J. M. Amador, Prof. D. A. Keszler, Prof. M. Nyman
Center for Sustainable Materials Chemistry (CSMC) and Department of Chemistry, Oregon State University
Corvallis, OR 97331-4003 (USA)
E-mail: may.nyman@oregonstate.edu
Homepage: http://nyman.chem.oregonstate.edu/
http://sustainablematerialschemistry.org/

Supporting information and the ORCID identification number(s) for the author(s) of this article can be found under http://dx.doi.org/10.1002/anie.201601134.

groups were not located in the electron density maps generated during the structure determination. Hence, the hydroxo assignment derives from balancing cluster and TMA charges and considering Hf-O distances. The average Hf–O distance, 2.25 Å, for terminal aqua ligands in $[Hf_4(OH)_8(H_2O)_{16}]^{8+}$ and $[Hf_6O_5(SO_4)_{10.5}(H_2O)_{6.5}]^{7-}$ is significantly longer (Table S1 in the Supporting Information),[7,13] than the average terminal Hf–O distance, 2.08 Å (Table S2), in **Hf_6**, indicating terminal hydroxo ligands. BVS values obtained from the terminal Hf–O bond lengths in **Hf_6** (0.69 average, Table S2) are also significantly larger than the values obtained from Hf–O bond lengths for terminal water ligands (0.44 average, Table S1). As indicated by O···O distances near 2.9 Å, hydrogen from these terminal hydroxo groups participate in H-bonding with the peroxide oxygen atoms from adjacent clusters (Figure 1, right) and with water molecules (not shown in Figure 1). All six TMA cations required to charge balance the $[Hf_6(\mu\text{-}O_2)_6(\mu\text{-}OH)_6(OH)_{12}]^{6-}$ anion were located in the structure analysis.

The presence of the peroxide ligand is confirmed by a signal at 835 cm^{-1} in the Raman spectrum of crystals, and the 1:1 Hf:O_2^{2-} ratio is verified by potassium permanganate titration (see Experimental Section 2 and Figure S1). The number of waters of crystallization could not be reliably quantified by TGA because the **Hf_6** crystals are hygroscopic. Thirty eight water molecules per hexamer were modeled in the crystal structure.

The **Hf_6** ring has been previously recognized as a part of a POM framework, where it is stabilized by three capping phosphodecatungstate ligands and K^+-cations.[25] The **Hf_6** ring, however, has not previously been isolated without the stabilization of these inorganic ligands. In the Hf-tungstate POM obtained at pH 4.8, instead of the terminal hydroxy ligands, the **Hf_6** cluster is capped by terminal oxo-ligands of the lacunary tungstate clusters. Notably, few polynuclear peroxo complexes of hafnium have been reported,[25–27] and all of them utililze well-known chemistry for the isolation of transition-metal and rare-earth substituted POMs. A series of hexanuclear peroxogermanate anions with a similar architecture to **Hf_6** were reported recently;[28] These clusters present end-on peroxide coordination to Ge rather than the side-on bridging in **Hf_6**; and the bridging ligands in the Ge_6 ring are oxo instead of hydroxo.

The radii of gyration R_g determined by Guinier approximation of the SAXS data for **Hf_6** solutions with varying concentration (Figure 2 and Table S3) are too large (6.5 to 9 Å) to represent only the **Hf_6** cluster, since $R_g = 3.8$ from simulated scattering for a single **Hf_6** cluster. Additionally, for all concentrations R_g increases with solution aging, reaching ca. 12 Å at 9 days for the lowest concentration **Hf_6** solution (Figure 2 and Table S3). The increase of the scattering intensity at $q < 0.1$ $Å^{-1}$ also indicates an increase in the average particle size with aging (Figures 3 and S2) suggesting that **Hf_6** undergoes oligomerization in solution. In the solid-state, the terminal hydroxo ligands of **Hf_6** assemble the clusters into chains via hydrogen bonding represented by O···O (Figure 1, right). To study a corresponding organization in solution, we compared our experimental data with the simulated data for chains of clusters directly derived from the

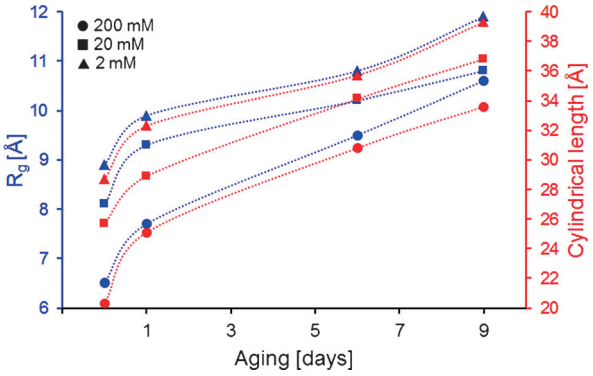

Figure 2. Calculated R_g (blue) from Guinier fits and cylindrical lengths (red) from cylindrical fits for **Hf_6**, crystals dissolved in water as a function of aging time and Hf concentration.

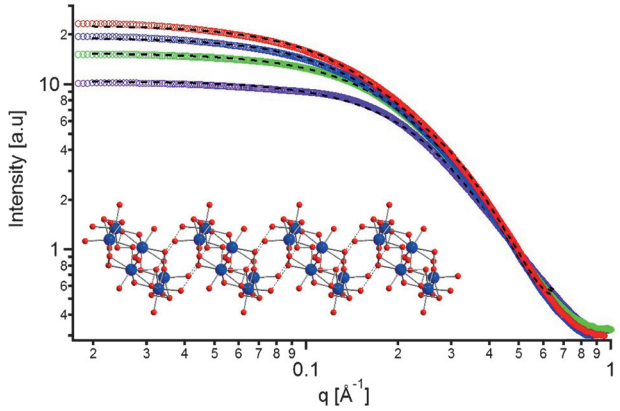

Figure 3. SAXS scattering curve for **Hf_6** crystals dissolved in water ([Hf] = 200 mM). The solution was aged for 0 (purple), 1 (green), 6 (blue) and 9 (red) days. Black dotted lines are cylindrical model fits to the experimental data (see Table S3 for model parameters). Inset: Representation of hydrogen bonded clusters of **Hf_6** forming chains.

structure (Table S3). The simulated R_g values for chains of three, four, and five clusters are 7.5, 9.6, and 11.6 Å (Table S3), respectively, which are very similar to the experimental values (Figure 2 and Table S3) that range between 6.5 and 11.9 Å. Moreover, the scattering data fit well to a cylindrical model with a radius of ca. 5.5 Å, which is similar to the radius of the **Hf_6** cluster (Figure 2 and Table S3). While the radius is invariant to aging and concentration, cylinder lengths vary between 20 and 39 Å (Figure 2 and Table S3), corresponding to chains with three to five clusters. As seen in Figure 2, lengths increase with aging and dilution. Dilution reduces counterion shielding and produces longer chains. Aging probably results in intercluster hydrolysis and condensation involving the terminal hydroxo. Aging does not produce changes in pH, and the peroxide Raman signature remains constant (Figure S1, right), confirming that the terminal hydroxo ligands, and not the peroxide groups, are responsible for the condensation reactions. Moreover, addition of TMAH to an aged solution of **Hf_6** did not produce any changes in the scattering curve (Figure S3), indicating that TMAH is not sufficient to reverse the polymerization.

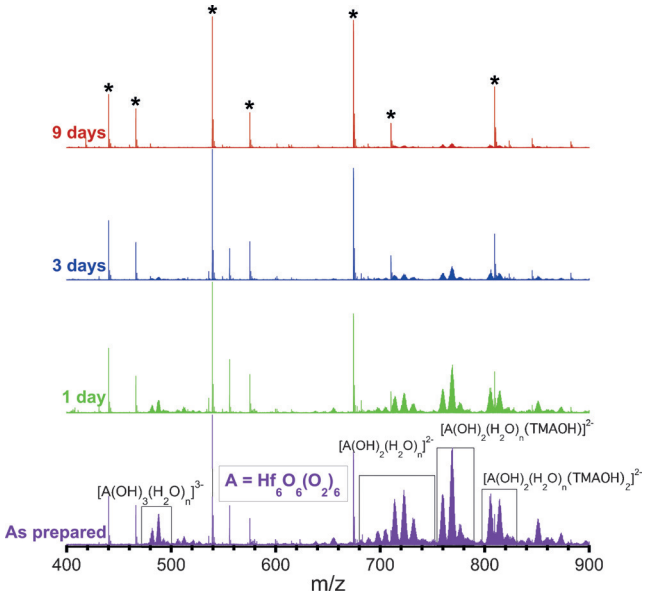

Figure 4. ESI-MS spectra of **Hf_6** crystals dissolved in water at selected aging times. Data are normalized to the strongest peak in each spectrum over the selected range. The asterisks indicate peaks associated with TMA-carbonate species formed by CO_2 absorption from the air. See Table S4 and Figure S4 for detailed peak assignments.

Figure 4 shows the labelled peak envelopes from ESI-MS analysis of **Hf_6** crystals dissolved in water (see Table S4 and Figure S4 for detailed peak assignments). The peak envelopes observed are consistent with hexameric species containing coordinated peroxide. The clusters detected have a general formula of $[Hf_6O_6(O_2)_6(OH)_x(H_2O)_n(TMAOH)_m]^{x-}$, meaning the core of the peroxo-Hf hexameric ring, $[Hf_6O_6(O_2)_6]$, is robust, while the hydroxo ligands are more labile in solution and with ionization-induced fragmentation. As the solution ages, the **Hf_6** peak intensity decreases; after nine days the cluster peaks have essentially disappeared. According to previous ESI-MS studies on hafnium-sulfate aqueous solutions, the ionization process may reject the larger polymeric species that evolve with solution aging.[4] Hence, the reduction of cluster peaks with aging time is consistent with the increase of oligomer size observed with SAXS. These observations are consistent with chain growth via oligomerization of the **Hf_6** clusters.

We also analyzed the crude $HfOCl_2$–TMAH–H_2O_2 reaction mixture ($pH \geq 14$). The same **Hf_6** clusters were detected by ESI-MS (Figure S5). At saturation, i.e., 3 days aging and right before **Hf_6** crystallization, the peak intensity decreases due to cluster oligomerization. SAXS data (Figure S6) suggests polydispersity (slope in low-q region $\neq 0$). Size distribution shows particles with mean diameters of 8, 16.5, and 28.5 Å (Figure S7), up to 4 clusters preassembled into chains just prior to crystallization.

The solid-state organization of the anionic clusters into chains by H-bonding correlates to similar order in aqueous solutions. SAXS confirms that **Hf_6** immediately forms elongated particles when dissolved in water, while ESI-MS demonstrates that the oligomers are formed from **Hf_6** monomers. This organization represents an emergent state for a condensed solid oxide. As such, it provides a unique system to study condensation thermally through the termal hydroxo ligands or photolytically through the peroxo ligands.

Here we have shown that similar hafnium clusters can exist at the extreme ends of the pH scale, i.e., <1 and >13. Although initial dissolution of Hf^{4+} cannot be performed without peroxide at high pH; it does not seem important in maintaining solubility, since it resides in an internal bridging position rather than a capping position. The inherently reactive nature of hydroxide ligands suggest these are not the origin of this unusual solubility and stability. However, the bulky and non-associating character of TMA counterions perhaps play a vital role, similar to the sulfate counterions and ligands of Hf-clusters in acid. TMA enables solubility, yet can be easily displaced by pyrolysis, oxidation, or ion exchange to produce HfO_2. Finally, this amphoteric speciation is key for realizing single-digit-nm lithographic resolution with radiation sensitive oxo-hydroxo metal clusters.

Acknowledgements

This material is based on work in the Center for Sustainable Materials Chemistry, which is supported by the U.S. National Science Foundation under Grant CHE-1102637. The single-crystal data were collected at the Advanced Photon source. ChemMatCARS Sector 15 is principally supported by the Divisions of Chemistry (CHE) and Materials Research (DMR), National Science Foundation, under grant number NSF/CHE-1346572. Use of the Advanced Photon Source, an Office of Science User Facility operated for the U.S. Department of Energy (DOE) Office of Science by Argonne National Laboratory, was supported by the U.S. DOE under Contract No. DE-AC02-06CH11357.

Keywords: cluster compounds · hafnium · mass spectrometry · peroxides · small-angle X-ray scattering

How to cite: *Angew. Chem. Int. Ed.* **2016**, *55*, 6221–6224
Angew. Chem. **2016**, *128*, 6329–6332

[1] L. B. Fullmer, R. H. Mansergh, L. N. Zakharov, D. A. Keszler, M. Nyman, *Cryst. Growth Des.* **2015**, *15*, 3885–3892.
[2] Z. L. Mensinger, J. T. Gatlin, S. T. Meyers, L. N. Zakharov, D. A. Keszler, D. W. Johnson, *Angew. Chem. Int. Ed.* **2008**, *47*, 9484–9486; *Angew. Chem.* **2008**, *120*, 9626–9628.
[3] S. W. Smith, W. Wang, D. A. Keszler, J. Conley, *J. Vac. Sci. Technol. A* **2014**, *32*, 041501.
[4] R. E. Ruther, B. M. Baker, J.-H. Son, W. H. Casey, M. Nyman, *Inorg. Chem.* **2014**, *53*, 4234–4242.
[5] R. P. Oleksak, R. E. Ruther, F. Luo, K. C. Fairley, S. R. Decker, W. F. Stickle, D. W. Johnson, E. L. Garfunkel, G. S. Herman, D. A. Keszler, *ACS Appl. Mater. Interfaces* **2014**, *6*, 2917–2921.
[6] C. F. Baes, R. E. Messmer, *The Hydrolysis of Cations*, Wiley, New York, **1976**.
[7] A. Kalaji, L. Soderholm, *Inorg. Chem.* **2014**, *53*, 11252–11260.
[8] W. Mark, M. Hansson, *Acta Crystallogr. Sect. B* **1975**, *31*, 1101–1108.
[9] S. J. Dalgarno, J. L. Atwood, C. L. Raston, *Inorg. Chim. Acta* **2007**, *360*, 1344–1348.

[10] A. Kalaji, L. Soderholm, *Chem. Commun.* **2014**, *50*, 997 – 999.
[11] Y. V. Kuznetsov, L. Dikareva, D. Rogachev, M. Porai-Koshits, *J. Struct. Chem.* **1984**, *26*, 923 – 929.
[12] C. Hagfeldt, V. Kessler, I. Persson, *Dalton Trans.* **2004**, 2142 – 2151.
[13] A. Kalaji, S. Skanthakumar, M. G. Kanatzidis, J. F. Mitchell, L. Soderholm, *Inorg. Chem.* **2014**, *53*, 6321 – 6328.
[14] J. T. Anderson, C. L. Munsee, C. M. Hung, T. M. Phung, G. S. Herman, D. C. Johnson, J. F. Wager, D. A. Keszler, *Adv. Funct. Mater.* **2007**, *17*, 2117 – 2124.
[15] P. D. Ashby, D. L. Olynick, D. F. Ogletree, P. P. Naulleau, *Adv. Mater.* **2015**, *27*, 5813 – 5819.
[16] J.-H. Son, D.-H. Park, D. A. Keszler, W. H. Casey, *Chem. Eur. J.* **2015**, *21*, 6727 – 6731.
[17] M. N. Jackson, M. K. Kamunde-Devonish, B. A. Hammann, L. A. Wills, L. B. Fullmer, S. E. Hayes, P. H. Cheong, W. H. Casey, M. Nyman, D. W. Johnson, *Dalton Trans.* **2015**, *44*, 16982 – 17006.
[18] Z. L. Mensinger, W. Wang, D. A. Keszler, D. W. Johnson, *Chem. Soc. Rev.* **2012**, *41*, 1019 – 1030.
[19] W. H. Casey, *Chem. Rev.* **2006**, *106*, 1 – 16.
[20] M. Nyman, P. C. Burns, *Chem. Soc. Rev.* **2012**, *41*, 7354 – 7367.
[21] M. Nyman, *Dalton Trans.* **2011**, *40*, 8049 – 8058.
[22] M. T. Pope, *Heteropoly and Isopoly Oxometalates*, Springer, Berlin, **1983**.
[23] M. T. Pope, A. Müller, *Angew. Chem. Int. Ed. Engl.* **1991**, *30*, 34 – 48; *Angew. Chem.* **1991**, *103*, 56 – 70.
[24] Crystallographic data for $[TMA]_6[Hf_6(\mu\text{-}O_2)_6(\mu\text{-}OH)_6\text{-}(OH)_{12}]\cdot 38H_2O$ (**Hf$_6$**) (Further details on the crystal structure investigations may be obtained from the Fachinformationszentrum Karlsruhe, 76344 Eggenstein-Leopoldshafen, Germany (fax: (+49) 7247-808-666; e-mail: crysdata@fiz-karlsruhe.de), on quoting the depository number CSD-430320): $C_{24}N_6O_{68}Hf_6$, $M_r = 2532.25\ g\,mol^{-1}$, dimensions $0.004 \times 0.032 \times 0.007\ mm^3$, triclinic, $P\bar{1}(2)$, $a = 7.788(3)$, $b = 16.290(6)$, $c = 18.616(7)$ Å, $\alpha = 73.533(7)$, $\beta = 81.812(8)$, $\gamma = 87.859(8)°$, $V = 2241.78(150)$ Å^3, $Z = 1$, $\rho_{calcd} = 1.87559\ g\,cm^{-3}$, $\mu = 1.572\ mm^{-1}$, radiation synchrotron, $\lambda = 0.41328$ Å, $T = 100(2)$ K, $2\theta_{max} = 17.771$, $F(000) = 1163$, $R_{all} = 0.1335$, R(reflections) = 0.0871(9634), $wR2$(reflections) = 0.2783(13902). Single crystal X-ray diffraction experiments were conducted at ChemMatCARS (sector 15) of the Advanced Photon Source (APS), Argonne National Laboratory (ANL). Data were collected using a Bruker D8 fixed-chi diffractometer equipped with an APEX II, CCD detector.
[25] B. S. Bassil, S. Mal, M. H. Dickman, U. Kortz, H. Oelrich, L. Walder, *J. Am. Chem. Soc.* **2008**, *130*, 6696 – 6697.
[26] S. Mal, N. H. Nsouli, M. Carraro, A. Sartorel, G. Scorrano, H. Oelrich, L. Walder, M. Bonchio, U. Kortz, *Inorg. Chem.* **2010**, *49*, 7 – 9.
[27] M. Carraro, N. Nsouli, H. Oelrich, A. Sartorel, A. Sorarù, S. Mal, G. Scorrano, L. Walder, U. Kortz, M. Bonchio, *Chem. Eur. J.* **2011**, *17*, 8371 – 8378.
[28] A. G. Medvedev, A. A. Mikhaylov, A. V. Churakov, M. V. Vener, T. A. Tripol'skaya, S. Cohen, O. Lev, P. V. Prikhodchenko, *Inorg. Chem.* **2015**, *54*, 8058 – 8065.

Received: February 1, 2016
Published online: April 20, 2016

